Erschienen in: Materials Horizons ; 6 (2019), 7. - S. 1497-1503
https://dx.doi.org/10.1039/C9MH00445A

Quantification of ion migration in $CH_3NH_3PbI_3$ perovskite solar cells by transient capacitance measurements†

Moritz H. Futscher,[a] Ju Min Lee,[a] Lucie McGovern,[a] Loreta A. Muscarella,[a] Tianyi Wang,[a] Muhammad Irfan Haider,[b] Azhar Fakharuddin,[b] Lukas Schmidt-Mende[b] and Bruno Ehrler*[a]

Ion migration in halide perovskite films leads to device degradation and impedes large scale commercial applications. We use transient ion-drift measurements to quantify activation energy, diffusion coefficient, and concentration of mobile ions in methylammonium lead triiodide ($MAPbI_3$) perovskite solar cells, and find that their properties change close to the tetragonal-to-orthorhombic phase transition temperature. We identify three migrating ion species which we attribute to the migration of iodide (I^-) and methylammonium (MA^+). We find that the concentration of mobile MA^+ ions is one order of magnitude higher than the one of mobile I^- ions, and that the diffusion coefficient of mobile MA^+ ions is three orders of magnitude lower than the one for mobile I^- ions in our samples. This quantification of mobile ions in $MAPbI_3$ will lead to a better understanding of ion migration and its role in operation and degradation of perovskite solar cells.

New concepts

Perovskite solar cells have been in the spotlight of the solar cell community in recent years due to their rapid increase in power conversion efficiency. However, ion migration in these perovskites leads to device degradation and changes the properties of the device during operation, both undesirable for applications. The understanding of ion migration is therefore crucial for the fabrication of stable and efficient perovskite devices. The measured properties of mobile ions vary widely across measurements and theoretical predictions in the literature. In addition, most experimental techniques fail to distinguish between the movement of cations and anions. We show that transient ion-drift is a fast and powerful method to quantity activation energy, diffusion coefficient, and concentration of mobile ions in perovskite solar cells. By studying methylammonium lead triiodide ($MAPbI_3$) we found that both MA^+ and I^- ions migrate at room temperature, but with very different diffusion coefficients (10^{-9} and 10^{-12} cm^2 s^{-1}). We furthermore observe that the activation energy of mobile I^- ions (0.29 ± 0.06 eV) is highly reproducible for different devices, while the activation energy of mobile MA^+ depends strongly on device fabrication. Our measurements offer quantitative insights and guide future theoretical investigations on ion migration in halide perovskites.

Introduction

Organic–inorganic metal halide perovskites have proven to be a promising candidate for low-cost photovoltaic devices. Due to their large charge-carrier diffusion length, long charge-carrier lifetime, and high defect tolerance, perovskite solar cells already reach record efficiencies greater than 23%, outperforming any other solution-processed solar cell technology.[1–4] Hybrid perovskites benefit from a continuously tunable bandgap, making them favorable for multi-junction devices with potential power conversion efficiencies above 30%.[5–8]

Unlike conventional inorganic solar cell materials, hybrid perovskites are ionic solids that exhibit ion migration, complicating the efficiency measurements and the definition of a steady-state condition in these cells.[9] This ion migration has also been shown to be a pathway for the degradation of perovskite solar cells.[10,11] The understanding of ion migration within perovskite solar cells is therefore crucial for the fabrication of stable perovskite devices.

In methylammonium lead triiodide ($MAPbI_3$), both anions (I^-) and cations (methylammonium MA^+, Pb^{2+}) can migrate due to the presence of vacancies, interstitials, or antisite substitutions. A large variety of activation energies for ion migration have been published, both measured experimentally and predicted theoretically. Theoretical calculations predict activation energies between 0.08 and 0.58 eV, 0.46 and 1.12 eV, and 0.80 and 2.31 eV for the migration of I^-, MA^+, and Pb^{2+}, respectively.[12–16] Attempts to experimentally determine the activation energy have given a similar variety of results.[17–24] Most experimental techniques further fail to distinguish between the charge of the ions (anions and cations), which can lead to mis-assignment of the ion species.

[a] *Center for Nanophotonics, AMOLF, Science Park 104, 1098 XG Amsterdam, The Netherlands. E-mail: ehrler@amolf.nl*
[b] *Department of Physics, University of Konstanz, Universitätsstraße 10, 78457 Konstanz, Germany*

Here we quantify the activation energy, diffusion coefficient, sign of charge, and concentration of mobile ions in $MAPbI_3$ using transient ion-drift, one of the most powerful methods to quantify ion migration.[25,26] We show that probing the capacitance change associated with ion migration requires to measure the capacitance transients on the timescale of seconds. Using transient ion-drift we identify footprints of distinct mobile ion species which we attribute to the migration of I^- (activation energy 0.29 eV) and MA^+ (0.39–0.90 eV). We find that the concentration of mobile MA^+ ions is one order of magnitude higher than the one of mobile I^- ions, and that the diffusion coefficient of mobile MA^+ ions is three orders of magnitude lower than the one for mobile I^- ions. As a result, the migration of MA^+ ions leads to a capacitance transient with a time scale of seconds, where the migration of I^- ions results in a transient with a time scale of less than a millisecond at 300 K. This quantification leads to a better understanding of ion migration, which is a crucial step towards stable perovskite solar cells.

Results and discussion

Transient ion-drift measurements rely on the external application of an electric field. We use a diode configuration to study ion migration. Our diode consists of an inverted planar perovskite solar cell architecture with a solution-processed NiO_x film as a hole-transporting layer and C_{60} as an electron-transport layer,[27] as shown in Fig. 1a. We chose the inverted solar cell structure over the standard one due to the strong tendency of the latter to accumulate charges, both electronic and ionic, at the TiO_2/perovskite interface resulting in a capacitive hysteresis and additional dielectric contributions, which is reduced in the inverted structure (see Section S1 in the ESI†).[28] In the inverted solar cell architecture, PEDOT:PSS (poly(3,4-ethylenedioxythiophene)–poly(styrenesulfonate)) is the most widely used hole-transport material, however, its high acidity and tendency to absorb water might lead to unwanted device degradation.[29] We furthermore avoid using spiro-MeOTAD (2,2′,7,7′-tetrakis[*N*,*N*-di(4-methoxyphenyl)amino]-9,9′-spirobifluorene) since typical dopants such as lithium salts lead to instabilities due to their high sensitivity to moisture, and can show misleading features in the transient ion-drift measurements due to the additional dopant ion migration.[30,31] The current–voltage characteristics of a perovskite solar cell in the dark in forward and reverse voltage scans are shown in Fig. 1b (see Fig. S3 in the ESI† for current–voltage characteristics measured at 1 sun). We observe a significant difference between the forward and reverse scanning direction at 300 K. When cooling the perovskite solar cell, this current–voltage hysteresis is strongly reduced and almost vanishes at 180 K (see inset Fig. 1b, and Fig. S4 in the ESI,† for current–voltage curves measured between 180 and 330 K). This has previously been attributed to the inhibition of the ion migration at low temperatures.[32,33]

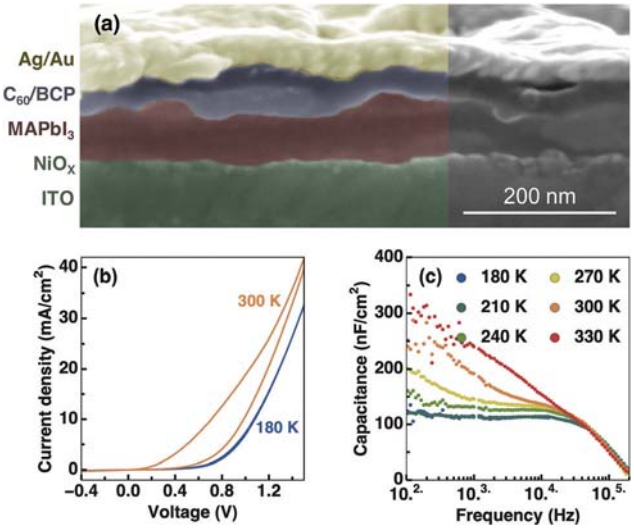

Fig. 1 Inverted $MAPbI_3$ device characteristics. (a) Cross-section scanning electron microscopy, (b) current–voltage characteristics measured in the dark, and (c) impedance spectroscopy measured in the dark at 0 V with an AC perturbation of 20 mV. The high capacitance at low frequencies is attributed to the high ionic conductivity mediated by defect states.

The transient ion-drift technique relies on probing the ion migration in the perovskite layer using capacitance transients at different temperatures. To find the suitable AC frequency regime for measuring capacitance transients, we study the frequency-dependence of the capacitance of the perovskite diode in the dark (see Fig. 1c). At low frequencies, the capacitance is dominated by mobile ions which accumulate near the contact interfaces.[34] When reducing the temperature, both the current–voltage hysteresis and the ionic capacitance contribution are strongly reduced until they disappear close to 180 K. At high frequencies, the capacitance is reduced due to the series resistance of the conductive contact layers reducing the cut-off frequency of the device. Between the two limits lies a relatively constant plateau, corresponding to the geometric capacitance of the device, which is related to the perovskite permittivity (see Section S3 in the ESI† for details).

We chose to measure the capacitance at 10 kHz, at the plateau of the capacitance. Transient ion-drift uses the transient capacitance response following a voltage pulse at different temperatures (see schematic Fig. 2). We apply a forward bias of 0.4 V for 1 second, which reduces the width of depletion region and leads to a new equilibrium distribution within the previously depleted region (Fig. 2a–c), changing the capacitance of the device. This change in capacitance did not increase further with longer pulse widths, indicating that a uniform distribution of ions was reached after the 1 second voltage pulse duration (see Fig. S6 in the ESI†).[25] We avoid using higher external voltages since Yuan *et al.* found that external electrical fields as low as 3 V μm^{-1} at 330 K can lead to the formation of PbI_2.[35] After turning off the voltage pulse, the built-in electric field will drive both the mobile ions and electric charges back to the contact interfaces (Fig. 2d). Mobile anions will follow the electrons and mobile cations will follow the holes, resulting in a capacitance transient. We measure this capacitance transient at temperatures between 180 and 350 K (see Fig. 3a), above the first-order phase transition from tetragonal to orthorhombic near 165 K.[36,37] We see no capacitance transient at low temperatures ($<$190 K), while a negative capacitance change

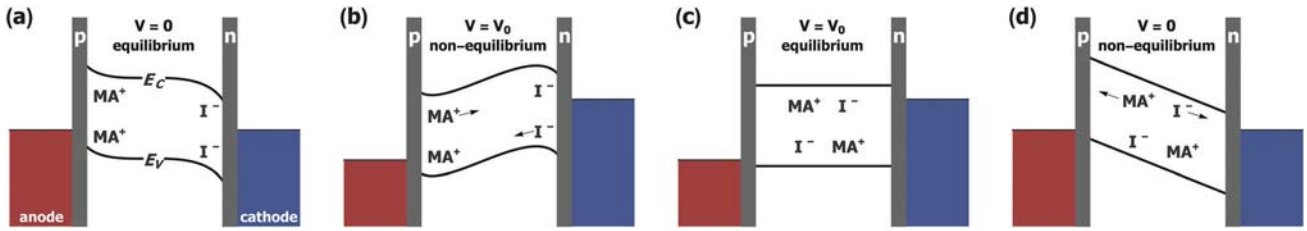

Fig. 2 Influence of ion migration on the band energies. (a) At short circuit, mobile MA^+ and I^- ions accumulate at the interface partially screening the built-in electric field. (b) When applying a forward bias (V_0), mobile ions will drift towards the bulk, (c) resulting in a uniform ion distribution within the perovskite layer. (d) After removing the forward bias, the built-in electric field will drive mobile ions towards the interfaces. This drift of mobile ions towards the interfaces results in a capacitance transient used to quantify ion migration. E_C is the conduction band energy, and E_V the valence band energy.

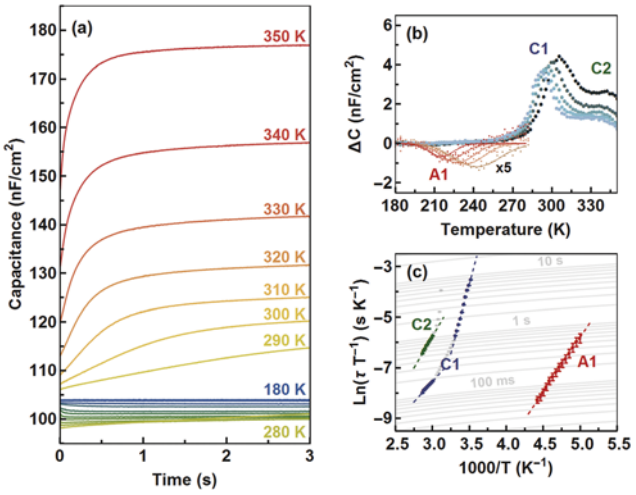

Fig. 3 Ion migration in $MAPbI_3$. (a) Capacitance transient measurements between 180 and 350 K with steps of 10 K measured at 0 V with an AC voltage of 10 mV at 10 kHz after a voltage pulse of 0.4 V for 1 second. (b) Rate-window plot of measured capacitance transients with different time constants ranging from milliseconds (red) to seconds (blue) reveal three ion species with different thermal emission rates. We attribute A1 to the migration of I^- ions and C1 and C2 to the migration of MA^+ ions. (c) Arrhenius plot of the observed thermal emission rates as a function of temperature. The linear fit reveals the activation energy and the diffusion coefficient of the mobile ion species.

grows in between 190 and 280 K until the capacitance decay it is too fast to measure. At higher temperatures, we observe a positive change in capacitance. Assuming the total ion concentration is conserved, the electric field varies linearly across the depletion region, and thermal diffusion of ions is negligible compared to ion drift, the change in capacitance depends only on the temperature, activation energy, diffusion coefficient, and concentration of mobile ions as[38]

$$C(t) = C(\infty) + \Delta C\left(1 - e^{-\frac{t}{\tau}}\right) \quad (1)$$

where ΔC is the change in capacitance due to the drift of mobile ions towards the interfaces, $C(\infty)$ the steady-state capacitance, and τ a time constant given by

$$\tau = \frac{k_B T \varepsilon_0 \varepsilon}{q^2 D N} \quad (2)$$

where k_B is the Boltzmann constant, and T the temperature, and N the doping density (see Section S5 in the ESI† for details). $D = \frac{\nu_0 d^2}{6} e^{-\frac{E_A}{k_B T}}$ is the ion-diffusion coefficient where ν_0 is the attempt-to-escape frequency of an ionic jump, d the jump distance, and E_A the activation energy.[39] The assumption that the electric field varies linearly across the depletion region is supported by recent studies showing that the electric field varies linearly within the perovskite layer when the perovskite layer is subjected to an external or internal electric field.[40,41] We can describe the measured capacitance transients using exponential functions, which further corroborates that the assumption of a linear field is valid in our devices (see Section S6 in the ESI†).[25] We note that Weber *et al.* found an additional interface dipole at the perovskite/SnO_2 interface.[40] This interface dipole is deliberately omitted in our structure by using NiO_x and C_{60} as extraction layers (see Section S1 in the ESI†). As metals are prone to reacting with I^- and mobile ions and can diffuse into the transport layers,[42,43] we have ensured to perform our measurements shortly after the fabrication of the diodes. In addition, we have carefully chosen the AC frequency to ensure that the measured capacitance is not affected by potential ion diffusion through the transport layers (see Section S7 in the ESI†).

To identify processes associated to the capacitance changes we use the rate window analysis, originally introduced by Lang to analyze deep-level transient spectroscopy (DLTS) measurements.[44] The capacitance change extracted by this method is given by $\Delta C = C(t_1) - C(t_2)$, where t_1 and t_2 depend on the typical decay times of the capacitance at a certain temperature to extract a peak associated with each activation energy. When choosing $t_1 = 2t_2$ from milliseconds to seconds we find three peaks corresponding to three separate processes, which we label A1, C1, and C2 (see Fig. 3b). The capacitance change associated with C1 and C2 both are positive and describe the migration of a cation. A1 is negative and describes the migration of an anion. We hence assign A1 to the migration of I^- ions and C1 and C2 to the migration of MA^+ ions. We exclude the migration of Pb^{2+} ions since theoretical studies suggest that they are unlikely to migrate.[16] Note that we cannot rule out the migration of H^+ ions, which was calculated to have an activation energy of 0.29 eV.[45] However, the predicted concentration of H^+ ions in $MAPbI_3$ is in the order of 10^{11} cm^{-3},[46] orders of magnitude lower than what we have measured.

The temperature dependence of the peaks in the rate window analysis together with their time scales can be used to obtain activation energy and diffusion coefficient of ion migration. This method, however, uses only two points of each transient to extract the time scales. To quantify ion migration using all data points, we fit the measured capacitance changes to exponential decays to obtain the time constants τ at different temperatures (eqn (1)). By means of an Arrhenius plot we can extract both the activation energy and diffusion coefficient (see Fig. 3c). We again identify the three species, C1, C2, and A1, where A1 occurs at much faster timescales and lower temperatures.

To estimate the sample-to-sample, and lab-to-lab variation we measured solar cells fabricated at AMOLF and at the University of Konstanz, with power conversion efficiencies ranging from 1 to 12% (see Section S9 in the ESI† for details). The obtained characteristics of mobile ions for all the devices are shown in Fig. 4 and the mean values are summarized in Table 1. We find that the activation energy for the migration of I^- ions is very reproducible across all devices, while the activation energy for the migration of MA^+ ions depends strongly on the fabrication conditions, which is consistent with the wide distribution of activation energies for the migration of MA^+ ions in the literature. The wide distribution of activation energies for the migration of I^- ions in the literature could be explained by the misinterpretation of mobile ion species, since most techniques cannot distinguish between the migration of anions and cations. The transient ion-drift measurements are able to simultaneously distinguish between mobile cations and anion, and detect low concentrations of mobile impurities ($\sim$0.01% of the doping density). Our measurements thus show that many theoretical calculations cannot be experimentally verified within the margin of error.

Interestingly, we obtain a diffusion coefficient of 10^{-9} cm^2 s^{-1} for I^- ions which is three orders of magnitude higher than the diffusion coefficient for MA^+ ions of 10^{-12} cm^2 s^{-1} (see Table 1). The diffusion coefficients measured here are very close to the diffusion coefficients measured with NMR (10^{-9} cm^2 s^{-1} for I^- and 10^{-15}–10^{-12} cm^2 s^{-1} for MA^+),[47,48] and to those obtained by Yuan *et al.* (4×10^{-11} cm^2 s^{-1} for MA^+),[18] Li *et al.* (5×10^{-8} to 6×10^{-9} cm^2 s^{-1} for I^-),[49] and Bertoluzzi *et al.* (8×10^{-9} cm^2 s^{-1} for I^-),[50] which supports our assignment of A1 to the migration of I^- ions and C1 and C2 to the migration of MA^+ ions. These values also suggest that the measured capacity change is due to the migration of ions and not to the migration of vacancies. Solute-dopant pairing can significantly slow down the ionic diffusion,[25] which could be the reason for the slow diffusion of MA^+ ions. Only the MA^+ ions have a transient decay time in the order of seconds at typical operation temperatures (<ms for I^-). Thus, our results suggest that mobile MA^+ ions are the origin of the observed current–voltage hysteresis in $MAPbI_3$ perovskite solar cells. Previously, also I^- has been assigned responsible for the current–voltage hysteresis,[16] however, the sensitivity of transient ion-drift to the sign of the ion excludes this possibility.

Close to the tetragonal-cubic phase-transition temperature (327 K)[46] we observe a decrease in activation energy and an increase in diffusion coefficient for one of the migrating MA^+ ions (C1) (with the exception for the device with a power conversion efficiency of 1%). A similar behavior has previously been observed and attributed to the volume change in the unit cell at temperatures close to the tetragonal-cubic phase transition.[51,52] Note that C2 might show a similar behavior at lower temperatures, however, the activation energy of C2 in the tetragonal phase could not be resolved in our measurements due to its long time constant. The obtained activation energies of the two migration pathways for MA^+ (C1 and C2) in the cubic phase are comparable, yet the diffusion coefficient of C1 is somewhat higher than the diffusion coefficient of C2. Using Kelvin probe force microscopy, Yun *et al.* found that ion migration near grain boundaries is much faster than inside the grains due to higher ionic diffusivity at grain boundaries.[53] We thus speculate that these are both mobile MA^+ species where C1 has a higher diffusion coefficient, which could be due to ion movement in vicinity of grain boundaries.

We measure the concentration of mobile ions from the change in capacitance following the voltage pulse. Since the capacitance $C(\infty) \propto \sqrt{N}$, the concentration of mobile ions N_{mobile} within the probed depletion region can be estimated as[54]

$$\left(\frac{\Delta C + C(\infty)}{C(\infty)}\right)^2 \propto \left(\frac{N_{\mathrm{mobile}} + N}{N}\right). \qquad (3)$$

The obtained concentrations for mobile I^- and MA^+ ions are summarized in Fig. 4c. We note that we assume a typical doping density of 1×10^{17} cm^{-3} for all the measured perovskite

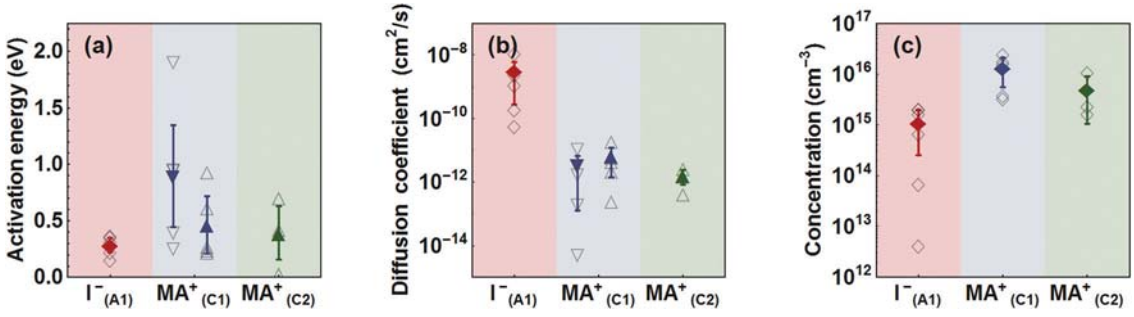

Fig. 4 Characteristics of mobile ions in $MAPbI_3$. (a) Activation energy, (b) diffusion coefficient at 300 K, (c) and concentration of mobile ions in $MAPbI_3$ perovskites obtained by transient ion-drift. The downward and the upward triangle represents measurements below and above the tetragonal-to-cubic phase-transition temperature. The mean values are summarized in Table 1.

Table 1 Characteristics of mobile ions in $MAPbI_3$

	A1	C1		C2
Migrating ion species	I^-	MA^+		MA^+
Charge	Negative	Positive		Positive
Concentration (cm^{-3})	$(1.1 \pm 0.9) \times 10^{15}$	$(1.3 \pm 0.8) \times 10^{16}$		$(5.0 \pm 4.0) \times 10^{15}$
Phase structure	Tetragonal	Tetragonal	Cubic	Cubic
Activation energy (eV)	0.29 ± 0.06	0.90 ± 0.45	0.46 ± 0.25	0.39 ± 0.24
Diffusion coefficient at 300 K ($cm^2\ s^{-1}$)	$(3.1 \pm 2.8) \times 10^{-9}$	$(3.4 \pm 3.3) \times 10^{-12}$	$(6.8 \pm 5.3) \times 10^{-12}$	$(1.6 \pm 0.8) \times 10^{-12}$

films and temperatures (see Section S3 in the ESI†).[55] Although the density of mobile ions depends on the fabrication, we find that the concentration of the mobile MA^+ ions is systematically about one order of magnitude higher than that of the mobile I^- ions. The measured mobile ion concentration is rather low compared to other studies, which report values of around 10^{18} cm^{-3}.[50] However, several recent studies measure a mobile ion concentration comparable to what we measure, on the order of 10^{15} cm^{-3},[40,41] suggesting that less than 10% of the screening of the electric field within the perovskite layer is produced by the presence of mobile ions. We note that electrical neutrality is still given, as the concentration obtained is the concentration of mobile ions within the perovskite film, not all ions present in the perovskite film.

Capacitance transients such as the ones observed here could also originate from deep-level charge traps. A powerful method to measure charge-carrier traps is DLTS,[44] a method which is very similar to transient ion-drift. DLTS has been used to study fast (<milliseconds) charge trapping in perovskite solar cells,[56] in contrast, ion migration in perovskites typically proceeds on long timescales of milliseconds to seconds.[57,58] Furthermore, the ratio of rise and decay times of the capacitance in DLTS and transient ion-drift is different, so that we can distinguish ion migration from trapping and de-trapping of charge carriers (see Section S8 in the ESI† for details).[26] We can therefore attribute the observed transients as the result of ion migration rather than deep-level charge traps. Atomistic simulations furthermore suggest that deep-level defects require high formation energies between 2 and 6 eV, such that their formation is unlikely.[1]

Conclusions

To conclude, we have shown that transient ion-drift is a fast and accurate method to quantify, with high precision, the activation energy, diffusion coefficient, sign of charge, and concentration of mobile ions in perovskite solar cells. In $MAPbI_3$ perovskites we observe that both MA^+ and I^- are migrating. We find that the concentration of mobile MA^+ ions is significantly higher than the concentration of mobile I^- ions in our samples and that the diffusion coefficient of I^- ions is three orders of magnitude higher than the diffusion coefficient of MA^+ ions. On timescales associated with current–voltage measurements, only the migration of MA^+ ions is slow enough to cause a current–voltage hysteresis in $MAPbI_3$ solar cells. The migration of I^- ions is still relevant for the device operation, and the degradation of perovskite solar cells. The migration of mobile I^- ions is very reproducible across devices fabricated in different laboratories, while the migration of mobile MA^+ ions strongly depends on the fabrication, which explains the wide distribution of activation energies for the migration of MA^+ ions in literature. Our measurements guide the future theoretical investigation into ion migration in halide perovskites and offer quantitative insight into the parameters of the mobile ion species, and hence the degradation pathways of perovskite solar cells.

Conflicts of interest

There are no conflicts to declare.

Acknowledgements

The authors thank Erik C. Garnett for carefully reading and commenting on the manuscript. M. I. H. acknowledges HEC Pakistan for IRSIP fellowship. This work is part of the research program of the Netherlands Organization for Scientific Research (NWO).

References

1 W. J. Yin, T. Shi and Y. Yan, Unusual Defect Physics in CH3NH3PbI3 Perovskite Solar Cell Absorber, *Appl. Phys. Lett.*, 2014, **104**(6), 063903, DOI: 10.1063/1.4864778.

2 A. Kojima, K. Teshima, Y. Shirai and T. Miyasaka, Organometal Halide Perovskites as Visible-Light Sensitizers for Photovoltaic Cells, *J. Am. Chem. Soc.*, 2009, **131**, 6050–6051, DOI: 10.1021/ja809598r.

3 A. Polman, M. Knight, E. C. Garnett, B. Ehrler and W. C. Sinke, Photovoltaic Materials – Present Efficiencies and Future Challenges, *Science*, 2016, **352**, 307, DOI: 10.1126/science.aad4424.

4 Q. Jiang, Z. Chu, P. Wang, X. Yang, H. Liu, Y. Wang, Z. Yin, J. Wu, X. Zhang and J. You, Planar-Structure Perovskite Solar Cells with Efficiency beyond 21%, *Adv. Mater.*, 2017, **29**, 1703852, DOI: 10.1002/adma.201703852.

5 M. T. Hörantner and H. J. Snaith, Predicting and Optimising the Energy Yield of Perovskite-on-Silicon Tandem Solar Cells under Real World Conditions, *Energy Environ. Sci.*, 2017, **10**(9), 1983–1993, DOI: 10.1039/c7ee01232b.

6 M. H. Futscher and B. Ehrler, Modeling the Performance Limitations and Prospects of Perovskite/Si Tandem Solar Cells under Realistic Operating Conditions, *ACS Energy Lett.*, 2017, **2**(9), 2089–2095, DOI: 10.1021/acsenergylett.7b00596.

7 A. Karani, L. Yang, S. Bai, M. H. Futscher, H. J. Snaith, B. Ehrler, N. C. Greenham and D. Di, Perovskite/Colloidal Quantum Dot Tandem Solar Cells: Theoretical Modeling

and Monolithic Structure, *ACS Energy Lett.*, 2018, **3**(4), 869–874, DOI: 10.1021/acsenergylett.8b00207.
8 M. H. Futscher and B. Ehrler, Efficiency Limit of Perovskite/Si Tandem Solar Cells, *ACS Energy Lett.*, 2016, **1**(4), 2–7, DOI: 10.1021/acsenergylett.6b00405.
9 H. J. Snaith, A. Abate, J. M. Ball, G. E. Eperon, T. Leijtens, N. K. Noel, S. D. Stranks, J. T.-W. Wang, K. Wojciechowski and W. Zhang, Anomalous Hysteresis in Perovskite Solar Cells, *J. Phys. Chem. Lett.*, 2014, **5**(9), 1511–1515, DOI: 10.1021/jz500113x.
10 V. Nandal and P. R. Nair, Predictive Modeling of Ion Migration Induced Degradation in Perovskite Solar Cells, *ACS Nano*, 2017, **11**(11), 11505–11512, DOI: 10.1021/acsnano.7b06294.
11 A. R. Bowring, L. Bertoluzzi, B. C. O'Regan and M. D. McGehee, Reverse Bias Behavior of Halide Perovskite Solar Cells, *Adv. Energy Mater.*, 2018, **8**, 1702365, DOI: 10.1002/aenm.201702365.
12 J. M. Azpiroz, E. Mosconi, J. Bisquert and F. De Angelis, Defect Migration in Methylammonium Lead Iodide and Its Role in Perovskite Solar Cell Operation, *Energy Environ. Sci.*, 2015, **8**(7), 2118–2127, DOI: 10.1039/C5EE01265A.
13 J. Haruyama, K. Sodeyama, L. Han and Y. Tateyama, First-Principles Study of Ion Diffusion in Perovskite Solar Cell Sensitizers, *J. Am. Chem. Soc.*, 2015, **137**(32), 10048–10051, DOI: 10.1021/jacs.5b03615.
14 S. Meloni, T. Moehl, W. Tress, M. Franckeviius, M. Saliba, Y. H. Lee, P. Gao, M. K. Nazeeruddin, S. M. Zakeeruddin and U. Rothlisberger, *et al.*, Ionic Polarization-Induced Current–Voltage Hysteresis in CH3NH3PbX3perovskite Solar Cells, *Nat. Commun.*, 2016, **7**, 10334, DOI: 10.1038/ncomms10334.
15 P. Delugas, C. Caddeo, A. Filippetti and A. Mattoni, Thermally Activated Point Defect Diffusion in Methylammonium Lead Trihalide: Anisotropic and Ultrahigh Mobility of Iodine, *J. Phys. Chem. Lett.*, 2016, **7**(13), 2356–2361, DOI: 10.1021/acs.jpclett.6b00963.
16 C. Eames, J. M. Frost, P. R. F. Barnes, B. C. O'Regan, A. Walsh and M. S. Islam, Ionic Transport in Hybrid Lead Iodide Perovskite Solar Cells, *Nat. Commun.*, 2015, **6**, 7497, DOI: 10.1038/ncomms8497.
17 C. Li, A. Guerrero, Y. Zhong and S. Huettner, Origins and Mechanisms of Hysteresis in Organometal Halide Perovskites, *J. Phys.: Condens. Matter*, 2017, **29**(19), 193001, DOI: 10.1088/1361-648X/aa626d.
18 Y. Yuan, J. Chae, Y. Shao, Q. Wang, Z. Xiao, A. Centrone and J. Huang, Photovoltaic Switching Mechanism in Lateral Structure Hybrid Perovskite Solar Cells, *Adv. Energy Mater.*, 2015, **5**(15), 1500615, DOI: 10.1002/aenm.201500615.
19 O. S. Game, G. J. Buchsbaum, Y. Zhou, N. P. Padture and A. I. Kingon, Ions Matter: Description of the Anomalous Electronic Behavior in Methylammonium Lead Halide Perovskite Devices, *Adv. Funct. Mater.*, 2017, **27**(16), 1606584, DOI: 10.1002/adfm.201606584.
20 A. Pockett, G. E. Eperon, N. Sakai, H. J. Snaith, L. M. Peter and P. J. Cameron, Microseconds, Milliseconds and Seconds: Deconvoluting the Dynamic Behaviour of Planar Perovskite Solar Cells, *Phys. Chem. Chem. Phys.*, 2017, **19**(8), 5959–5970, DOI: 10.1039/C6CP08424A.
21 T. Y. Yang, G. Gregori, N. Pellet, M. Grätzel and J. Maier, The Significance of Ion Conduction in a Hybrid Organic-Inorganic Lead-Iodide-Based Perovskite Photosensitizer, *Angew. Chem., Int. Ed.*, 2015, **54**(27), 7905–7910, DOI: 10.1002/anie.201500014.
22 J. Xing, Q. Wang, Q. Dong, Y. Yuan, Y. Fang and J. Huang, Ultrafast Ion Migration in Hybrid Perovskite Polycrystalline Thin Films under Light and Suppression in Single Crystals, *Phys. Chem. Chem. Phys.*, 2016, **18**(44), 30484–30490, DOI: 10.1039/C6CP06496E.
23 H. Yu, H. Lu, F. Xie, S. Zhou and N. Zhao, Native Defect-Induced Hysteresis Behavior in Organolead Iodide Perovskite Solar Cells, *Adv. Funct. Mater.*, 2016, **26**(9), 1411–1419, DOI: 10.1002/adfm.201504997.
24 D. W. DeQuilettes, W. Zhang, V. M. Burlakov, D. J. Graham, T. Leijtens, A. Osherov, V. Bulović, H. J. Snaith, D. S. Ginger and S. D. Stranks, Photo-Induced Halide Redistribution in Organic-Inorganic Perovskite Films, *Nat. Commun.*, 2016, **7**, 11683, DOI: 10.1038/ncomms11683.
25 T. Heiser and E. Weber, Transient Ion-Drift-Induced Capacitance Signals in Semiconductors, *Phys. Rev. B: Condens. Matter Mater. Phys.*, 1998, **58**(7), 3893–3903, DOI: 10.1103/PhysRevB.58.3893.
26 T. Heiser and A. Mesli, Determination of the Copper Diffusion Coefficient in Silicon from Transient Ion-Drift, *Appl. Phys. A: Solids Surf.*, 1993, **57**(4), 325–328, DOI: 10.1007/BF00332285.
27 X. Yin, Z. Yao, Q. Luo, X. Dai, Y. Zhou, Y. Zhang, Y. Zhou, S. Luo, J. Li and N. Wang, *et al.*, High Efficiency Inverted Planar Perovskite Solar Cells with Solution-Processed NiO*x* Hole Contact, *ACS Appl. Mater. Interfaces*, 2017, **9**(3), 2439–2448, DOI: 10.1021/acsami.6b13372.
28 G. Garcia-Belmonte and J. Bisquert, Distinction between Capacitive and Noncapacitive Hysteretic Currents in Operation and Degradation of Perovskite Solar Cells, *ACS Energy Lett.*, 2016, **14**, 683–688, DOI: 10.1021/acsenergylett.6b00293.
29 J. R. Manders, S. W. Tsang, M. J. Hartel, T. H. Lai, S. Chen, C. M. Amb, J. R. Reynolds and F. So, Solution-Processed Nickel Oxide Hole Transport Layers in High Efficiency Polymer Photovoltaic Cells, *Adv. Funct. Mater.*, 2013, **23**(23), 2993–3001, DOI: 10.1002/adfm.201202269.
30 Y. Zhang, M. Liu, G. E. Eperon, T. C. Leijtens, D. McMeekin, M. Saliba, W. Zhang, M. de Bastiani, A. Petrozza and L. M. Herz, *et al.*, Charge Selective Contacts, Mobile Ions and Anomalous Hysteresis in Organic–inorganic Perovskite Solar Cells, *Mater. Horiz.*, 2015, **2**(3), 315–322, DOI: 10.1039/C4MH00238E.
31 Q. Luo, Y. Zhang, C. Liu, J. Li, N. Wang and H. Lin, Iodide-Reduced Graphene Oxide with Dopant-Free Spiro-OMeTAD for Ambient Stable and High-Efficiency Perovskite Solar Cells, *J. Mater. Chem. A*, 2015, **3**(31), 15996–16004, DOI: 10.1039/C5TA02710A.
32 R. T. Ginting, E.-S. Jung, M.-K. Jeon, W.-Y. Jin, M. Song and J.-W. Kang, Low-Temperature Operation of Perovskite Solar Cells: With Efficiency Improvement and Hysteresis-Less, *Nano Energy*, 2016, **27**, 569–576, DOI: 10.1016/J.NANOEN.2016.08.016.
33 A. Bruno, D. Cortecchia, X. Y. Chin, K. Fu, P. P. Boix, S. Mhaisalkar and C. Soci, Temperature and Electrical Poling Effects on Ionic Motion in $MAPbI_3$ Photovoltaic Cells, *Adv. Energy Mater.*, 2017, **7**(18), 1700265, DOI: 10.1002/aenm.201700265.

34 O. Almora, I. Zarazua, E. Mas-Marza, I. Mora-Sero, J. Bisquert and G. Garcia-Belmonte, Capacitive Dark Currents, Hysteresis, and Electrode Polarization in Lead Halide Perovskite Solar Cells, *J. Phys. Chem. Lett.*, 2015, **6**(9), 1645–1652, DOI: 10.1021/acs.jpclett.5b00480.

35 Y. Yuan, Q. Wang, Y. Shao, H. Lu, T. Li, A. Gruverman and J. Huang, Electric-Field-Driven Reversible Conversion between Methylammonium Lead Triiodide Perovskites and Lead Iodide at Elevated Temperatures, *Adv. Energy Mater.*, 2016, **6**(2), 1501803, DOI: 10.1002/aenm.201501803.

36 M. T. Weller, O. J. Weber, P. F. Henry, A. M. Di Pumpo and T. C. Hansen, Complete Structure and Cation Orientation in the Perovskite Photovoltaic Methylammonium Lead Iodide between 100 and 352 K, *Chem. Commun.*, 2015, **51**(20), 4180–4183, DOI: 10.1039/C4CC09944C.

37 N. Onoda-Yamamuro, O. Yamamuro, T. Matsuo and H. Suga, P-T Phase Relations of $CH_3NH_3PbX_3$ (X = Cl, Br, I) Crystals, *J. Phys. Chem. Solids*, 1992, **53**(2), 277–281, DOI: 10.1016/0022-3697(92)90056-J.

38 A. Zamouche, T. Heiser and A. Mesli, Investigation of Fast Diffusing Impurities in Silicon by a Transient Ion Drift Method, *Appl. Phys. Lett.*, 1995, **66**(5), 631, DOI: 10.1063/1.114142.

39 D. Meggiolaro, E. Mosconi and F. De Angelis, Formation of Surface Defects Dominates Ion Migration in Lead-Halide Perovskites, *ACS Energy Lett.*, 2019, **4**(3), 779–785, DOI: 10.1021/acsenergylett.9b00247.

40 S. A. L. Weber, I. M. Hermes, S.-H. Turren-Cruz, C. Gort, V. W. Bergmann, L. Gilson, A. Hagfeldt, M. Graetzel, W. Tress and R. Berger, How the Formation of Interfacial Charge Causes Hysteresis in Perovskite Solar Cells, *Energy Environ. Sci.*, 2018, **11**(9), 2404–2413, DOI: 10.1039/C8EE01447G.

41 S. T. Birkhold, J. T. Precht, H. Liu, R. Giridharagopal, G. E. Eperon, L. Schmidt-Mende, X. Li and D. S. Ginger, Interplay of Mobile Ions and Injected Carriers Creates Recombination Centers in Metal Halide Perovskites under Bias, *ACS Energy Lett.*, 2018, **3**(6), 1279–1286, DOI: 10.1021/acsenergylett.8b00505.

42 E. Bi, H. Chen, F. Xie, Y. Wu, W. Chen, Y. Su, A. Islam, M. Grätzel, X. Yang and L. Han, Diffusion Engineering of Ions and Charge Carriers for Stable Efficient Perovskite Solar Cells, *Nat. Commun.*, 2017, **8**, 15330, DOI: 10.1038/ncomms15330.

43 S. Wang, Y. Kato, Y. Qi, S. R. Raga, M. V. Lee and L. K. Ono, Silver Iodide Formation in Methyl Ammonium Lead Iodide Perovskite Solar Cells with Silver Top Electrodes, *Adv. Mater. Interfaces*, 2015, **2**(13), 1500195, DOI: 10.1002/admi.201500195.

44 D. V. Lang, Deep-Level Transient Spectroscopy: A New Method to Characterize Traps in Semiconductors, *J. Appl. Phys.*, 1974, **45**(7), 3023–3032, DOI: 10.1063/1.1663719.

45 D. A. Egger, L. Kronik and A. M. Rappe, Theory of Hydrogen Migration in Organic–Inorganic Halide Perovskites, *Angew. Chem., Int. Ed.*, 2015, **54**(42), 12437–12441, DOI: 10.1002/anie.201502544.

46 J. M. Frost and A. Walsh, What Is Moving in Hybrid Halide Perovskite Solar Cells?, *Acc. Chem. Res.*, 2016, 528–535, DOI: 10.1021/acs.accounts.5b00431.

47 A. Senocrate, I. Moudrakovski, G. Y. Kim, T.-Y. Yang, G. Gregori, M. Grätzel and J. Maier, The Nature of Ion Conduction in Methylammonium Lead Iodide: A Multimethod Approach, *Angew. Chem., Int. Ed.*, 2017, **56**(27), 7755–7759, DOI: 10.1002/anie.201701724.

48 A. Senocrate, I. Moudrakovski, T. Acartürk, R. Merkle, G. Y. Kim, U. Starke, M. Grätzel and J. Maier, Slow CH_3NH_3 + Diffusion in $CH_3NH_3PbI_3$ under Light Measured by Solid-State NMR and Tracer Diffusion, *J. Phys. Chem. C*, 2018, **27**, 21803–21806, DOI: 10.1021/acs.jpcc.8b06814.

49 C. Li, A. Guerrero, S. Huettner and J. Bisquert, Unravelling the Role of Vacancies in Lead Halide Perovskite through Electrical Switching of Photoluminescence, *Nat. Commun.*, 2018, **9**(1), 5113, DOI: 10.1038/s41467-018-07571-6.

50 L. Bertoluzzi, R. A. Belisle, K. A. Bush, R. Cheacharoen, M. D. McGehee and B. C. O'Regan, *In Situ* Measurement of Electric-Field Screening in Hysteresis-Free PTAA/$FA_{0.83}Cs_{0.17}$-$Pb(I_{0.83}Br_{0.17})_3$/C_{60} Perovskite Solar Cells Gives an Ion Mobility of $\sim 3 \times 10^{-7}$ cm^2 V^{-1} s^{-1}, 2 Orders of Magnitude Faster than Reported for Metal–Oxide-Contacted, *J. Am. Chem. Soc.*, 2018, **140**(40), 12775–12784, DOI: 10.1021/jacs.8b04405.

51 M. Bag, L. A. Renna, R. Y. Adhikari, S. Karak, F. Liu, P. M. Lahti, T. P. Russell, M. T. Tuominen and D. Venkataraman, Kinetics of Ion Transport in Perovskite Active Layers and Its Implications for Active Layer Stability, *J. Am. Chem. Soc.*, 2015, **137**(40), 13130–13137, DOI: 10.1021/jacs.5b08535.

52 M. N. F. Hoque, N. Islam, Z. Li, G. Ren, K. Zhu and Z. Fan, Ionic and Optical Properties of Methylammonium Lead Iodide Perovskite across the Tetragonal–Cubic Structural Phase Transition, *ChemSusChem*, 2016, **9**(18), 2692–2698, DOI: 10.1002/cssc.201600949.

53 J. S. Yun, J. Seidel, J. Kim, A. M. Soufiani, S. Huang, J. Lau, N. J. Jeon, S. I. Seok, M. A. Green and A. Ho-Baillie, Critical Role of Grain Boundaries for Ion Migration in Formamidinium and Methylammonium Lead Halide Perovskite Solar Cells, *Adv. Energy Mater.*, 2016, **6**(13), 1600330, DOI: 10.1002/aenm.201600330.

54 I. Lyubomirsky, M. K. Rabinal and D. Cahen, Room-Temperature Detection of Mobile Impurities in Compound Semiconductors by Transient Ion Drift, *J. Appl. Phys.*, 1997, **81**(10), 6684–6691, DOI: 10.1063/1.365563.

55 O. Almora, C. Aranda, E. Mas-Marzá and G. Garcia-Belmonte, On Mott-Schottky Analysis Interpretation of Capacitance Measurements in Organometal Perovskite Solar Cells, *Appl. Phys. Lett.*, 2016, **109**(17), 173903, DOI: 10.1063/1.4966127.

56 S. Heo, G. Seo, Y. Lee, D. Lee, M. Seol, J. Lee, J.-B. Park, K. Kim, D.-J. Yun and Y. S. Kim, *et al.*, Deep Level Trapped Defect Analysis in $CH_3NH_3PbI_3$ Perovskite Solar Cells by Deep Level Transient Spectroscopy, *Energy Environ. Sci.*, 2017, **10**(5), 1128–1133, DOI: 10.1039/C7EE00303J.

57 R. S. Sanchez, V. Gonzalez-Pedro, J. W. Lee, N. G. Park, Y. S. Kang, I. Mora-Sero and J. Bisquert, Slow Dynamic Processes in Lead Halide Perovskite Solar Cells. Characteristic Times and Hysteresis, *J. Phys. Chem. Lett.*, 2014, **5**(13), 2357–2363, DOI: 10.1021/jz5011187.

58 R. Gottesman, E. Haltzi, L. Gouda, S. Tirosh, Y. Bouhadana, A. Zaban, E. Mosconi and F. De Angelis, Extremely Slow Photoconductivity Response of $CH_3NH_3PbI_3$ Perovskites Suggesting Structural Changes under Working Conditions, *J. Phys. Chem. Lett.*, 2014, **5**(15), 2662–2669, DOI: 10.1021/jz501373f.